To appear in *Molecular Simulation*
Vol. 00, No. 00, Month 20XX, 1–12

Citation
Aghajamali, A. and de Tomas, C. and Suarez-Martinez, I. and Marks, N. 2018. Unphysical nucleation of diamond in the extended cutoff Tersoff potential. Molecular Simulation. 44 (2): pp. 164-171. http://doi.org/10.1080/08927022.2017.1355555

FULL PAPER

Unphysical nucleation of diamond in the extended cutoff Tersoff potential

Alireza Aghajamali, Carla de Tomas, Irene Suarez-Martinez, and Nigel A. Marks*

Department of Physics and Astronomy, Curtin University, Perth WA 6102, Australia

(*May 23, 2017*)

In simulations of carbon materials it is common practice to view the coefficients of the cutoff function as free parameters which can be optimized according to the system of interest. This work examines a common modification to the widely-used Tersoff potential in which the coefficient of the upper cutoff is increased to improve the properties of amorphous carbon. Using Molecular Dynamics simulations, we show that this so-called Extended Cutoff Tersoff model leads to nucleation of diamond nanocrystals during annealing of amorphous carbon. By varying the density of the system, and examining the radial distribution function in conjunction with the modified cutoff function, we demonstrate that this behaviour is unphysical, and does not represent a new pathway for synthesizing diamond. Viewed from a broader perspective, this observation provides a cautionary tale against altering the parameters of empirical potentials without fully considering the wider implications.

Keywords: Molecular dynamics; Tersoff potential; Cutoff function; Diamond

1. Introduction

When Tersoff developed the first useful interatomic potential for carbon in 1988 [1], a new era in computational carbon science commenced. Based on a bond-order formalism proposed several years earlier by Abell [2], the Tersoff potential was the first empirical potential capable of describing the multiple hybridization states of carbon. With a straightforward functional form and low computational cost, the Tersoff potential found widespread use across the entire spectrum of carbon materials, including graphite, diamond, fullerenes, nanotubes and amorphous carbon. Presently around 1200 articles cite the original work.

Despite its utility, the Tersoff potential has some shortcomings: there is no long-range attraction between graphitic planes, nor is there a dihedral term to penalize rotation of π-bonds. Historically, one of the most significant improvements was the Reactive Empirical Bond-Order (REBO) potential developed by Brenner in 1990 [3], and since then around 40 carbon potentials have been proposed, most of which can trace their lineage to the original Tersoff model. For a discussion of the history of carbon potentials and a comparison of the merits of the dominant models, see Ref. [4].

The computational efficiency of the Tersoff potential arises from the short-range nature of the potential, in which nearest-neighbour contributions dominate. A central component of this short-range behaviour is the cutoff function, which varies smoothly from unity to zero according to the functional form:

$$f_c(r) = \begin{cases} 1 & r \leq R \\ \frac{1}{2} + \frac{1}{2}\cos\left[\pi(r-R)/(S-R)\right] & R < r < S \\ 0 & r \geq S \end{cases} \quad (1)$$

*Corresponding author. Email: N.Marks@curtin.edu.au

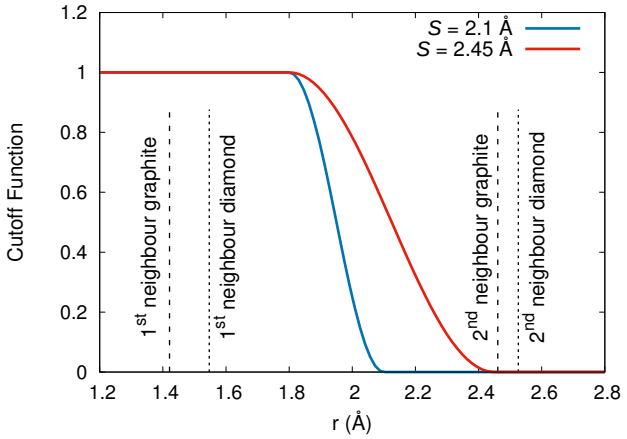

Figure 1. Cutoff function for the Tersoff potential (see Eq. 1) using the original parameters (blue curve, S=2.1 Å), and the Extended Cutoff Tersoff potential (red curve, S=2.45 Å). Dotted lines indicate the interatomic distances for the first and second coordination shells in graphite and diamond.

where r is the interatomic distance, R=1.8 Å and S=2.1 Å. The corresponding cutoff function is shown by the blue curve in Figure 1. Exactly the same cutoff function is used in the REBO potential, except with slightly different parameters (R=1.7 and S=2.0 Å).

For the main crystalline forms of carbon, i.e. graphite and diamond, the precise values of R and S do not affect bondlengths, elastic constants or cohesive energies. As long as R exceeds the nearest neighbour bondlength, and S is below the second neighbour bondlength, varying R and S does not alter properties of these bulk phases. As a result, the cutoff parameters are often considered as free parameters which can be tuned according to the task at hand. There are numerous examples of this philosophy with both the Tersoff and REBO family of potentials, particularly for studies of fracture and amorphous carbon. In the case of fracture simulations, the majority of which involve defects and grain boundaries in graphene, it is common to use a step-function cutoff (i.e. set $R = S$) to avoid non-physical strain hardening in stress-strain curves [5, 6]. As an aside, this practice should be strongly discouraged, as it results in discontinuous energies and forces, and alters the dynamics of bond rupture as detailed in Table S1 of the study by Gamboa *et al.* [7]. Fracture simulations typically use only a single value of the cutoff; values employed in the literature include: 1.92 Å [8–11], 1.95 Å [12], 2.0 Å [13–16] and 2.1 Å [17]. In studies of amorphous carbon, a variety of modifications have been employed, mostly motivated by the desire to increase the sp^3 fraction at high densities. In simulations using the REBO potential, Jäger and Albe [18] chose values of R=1.95 Å and S=2.25 Å, while Titantah and Lamoen [19] and Sha *et al.* [20] each performed Tersoff simulations leaving the original value of R unchanged, but with S increased to 2.45 Å. The cutoff function for this case is shown by the red line in Figure 1. A very similar value of S=2.46 Å was also proposed by Nordlund *et al.* [21] in an extension of the Tersoff potential to include van der Waals attraction.

In this work we use Molecular Dynamics (MD) simulations to explore the ramifications of increasing the cutoff of the Tersoff potential. We focus on the modification suggested in Refs. [19, 20] for amorphous carbon, in which R is unchanged and S=2.45 Å. Using a variety of values of S spanning the range 2.1 to 2.45 Å we construct amorphous carbon structures using the liquid quenching method [22] and subsequently anneal at high temperature. For the largest cutoff we observe unphysical nucleation of diamond at certain densities. Using the radial distribution function, we correlate this effect to interactions between the second neighbour coordination shell and the cutoff itself. This observation demonstrates that Tersoff potential with an extended cutoff is not as robust as has been assumed.

2. Methodology

Our MD simulations are performed using the LAMMPS software [23], and are broadly similar to our recent article [4] in which we compared the performance of six common potentials. The first step involves choosing a value of S, and making the appropriate change in the parameter file for the Tersoff potential. Four values of S are considered: 2.1, 2.2, 2.3 and 2.45 Å. The original value of R=1.8 Å is left unchanged.

For each value of the cutoff S, amorphous carbon networks are created for a variety of densities between 1.5 and 3.2 g/cc. To create the amorphous structure, a liquid is first created at the desired density, and then quenched to 300 K in 1 ps to form the amorphous solid. The liquid is generated via the spontaneous melting of a randomized simple cubic lattice, and is equilibrated at 9000 K for 5 ps. In our recent study of the unmodified Tersoff potential a temperature of 8000 K was used to equilibrate the liquid; this rather high value is necessary as the melting point of carbon with the original Tersoff potential is around 6000 K, an overestimate of roughly 2000 K [1]. For the values of S used in this work we find that an even higher value of 9000 K is required to ensure a highly diffusive liquid as measured by the mean-squared-displacement (MSD). An example plot of the MSD for S=2.45 Å at a density of 3 g/cc is shown in Figure 2(a); the MSD increases linearly with time and has a significant slope, indicative of a fully equilibrated liquid.

Once the amorphous structure is created, it is annealed for 400 ps at a temperature of 6000 K. This approach is identical in spirit to our recent article [4] in which high-temperature annealing was used to study structural evolution and transformation. As with the liquid, the MSD is used to select the annealing temperature, but in this case the goal is to have some atomic motion without melting the structure. Panel (b) of Figure 2 shows representative data of the MSD for annealing of the same 3 g/cc system shown in panel (a). In this case the MSD increases with time in a sub-linear manner, and the average absolute displacement (computed by taking the square-root of the MSD) is less than 3 Å after 400 ps. This demonstrates that there is rearrangement without the structure becoming a liquid.

After annealing, the structures are minimized to zero Kelvin and structural analysis is performed. Coordination analysis was performed by counting the number of nearest neighbours using a cutoff of 1.85 Å. For the purposes of analysis and visualization, atoms are considered to be sp, sp^2 and sp^3 hybridized if they have two, three and four neighbours, respectively. Diamond crystallites are identified using the diamond structure indentification tool [24] in the OVITO visualization package [25]. Atoms are classified as diamond if all of their first and second neighbours are positioned on diamond lattice sites (either cubic of hexagonal). If some of the second neighbours are absent, atoms are still counted as diamond if all four neighbours are positioned on a lattice site.

The simulations are performed in the NVT ensemble (meaning constant number of particles, volume and temperature) using the Bussi thermostat [26] to control the temperature. The equations of motion are integrated using the velocity Verlet algorithm and a time step of 0.1 fs is used. All simulations contain 32,768 atoms in a cubic simulation with periodic boundary conditions in all three dimension. The magnitude of the randomization used to destabilize the simple cubic lattice is 0.2 Å. Without this random displacement the atoms will not move since the

3. Results and Discussion

Using the technique outlined in the Methodology, amorphous carbon structure were created for a range of densities from 1.5 to 3.2 g/cc. It is well-known experimentally that the sp^3 fraction of amorphous carbon should vary linearly with density, and hence this relationship is a useful measure of the quality of a calculation. Figure 3 presents the sp^3 fraction of these amorphous carbons and for a range of densities and values of the cutoff S. For the original value of S, namely 2.1 Å, the sp^3 fraction differs substantially from experimental values shown as black circles. The discrepancy

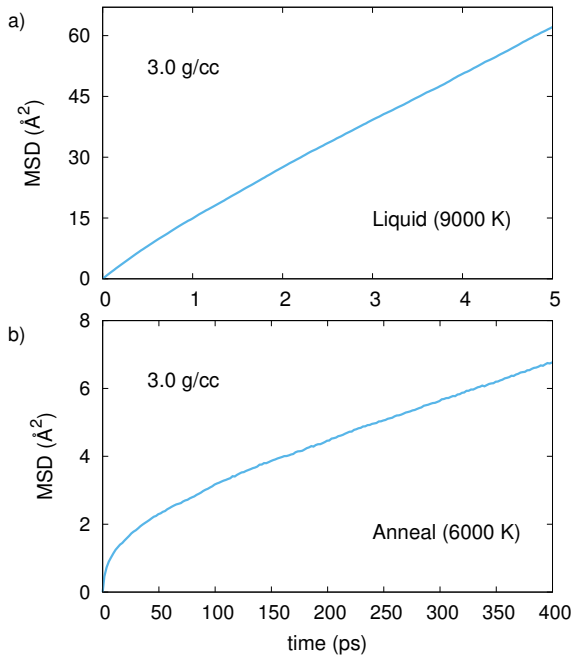

Figure 2. Representative data showing the mean-squared-displacement (MSD) as a function of time for S=2.45 Å and a density of 3 g/cc. a) Diffusion of the liquid at 9000 K, and b) Diffusion associated with structural evolution during annealing at 6000 K.

is particularly large at high densities, where the sp^3 fraction is underestimated by around a factor of two. Increasing the value of S doesn't change the sp^3 fraction at the lowest two densities, but for all other densities an effect is seen, particular at the highest density of 3.2 g/cc and largest value of S. In this case the sp^3 fraction rises to ∼75%, very close to the experimental value. This improvement in the sp^3 fraction of high density amorphous carbon is the reason that larger values of S have been proposed by previous authors [19, 20].

The next step in the simulations is the annealing of the amorphous carbon structures for long time to study structural evolution. Our original aim in performing these simulations was simply an exercise in benchmarking the performance of the modified Tersoff potential. Based on our experience with the original Tersoff potential, the expected behaviour was that the annealed carbons would closely resemble the parent structure, remaining amorphous and retaining similar coordination fractions. However, to our surprise we found that in some cases diamond crystals gradually appeared within the amorphous matrix. An example of one such simulation is shown in Figure 4 where S=2.45 Å and the density is 2.8 g/cc. The initial structure seen in panel (a) is the amorphous carbon structure, and the network is seen to be fully disordered, as shown by the colouring which depicts the hybridization state (red is sp, green is sp^2 and blue is sp^3). The remaining panels depict varying stages in the annealing, which is performed at 6000 K. At first very little change is discernible, but after 50 ps a small region of blue can be seen near the centre of the slice. These atoms are all sp^3 hybridized, and furthermore, the angle of the cross-sectional slice reveals the characteristic hexagonal channels of diamond. As the annealing continues, this crystallite continues to grow, and additional crystallites appear in the simulation cell, though not always with the

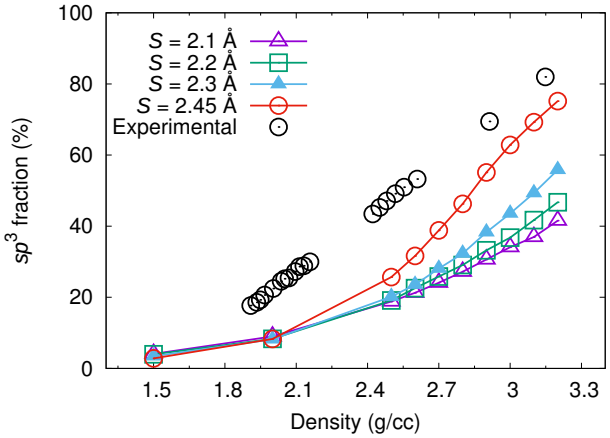

Figure 3. Amorphous carbon sp^3 fraction as a function of density for different values of the cutoff parameter S. Experimental data is from Schwan *et al.* [27].

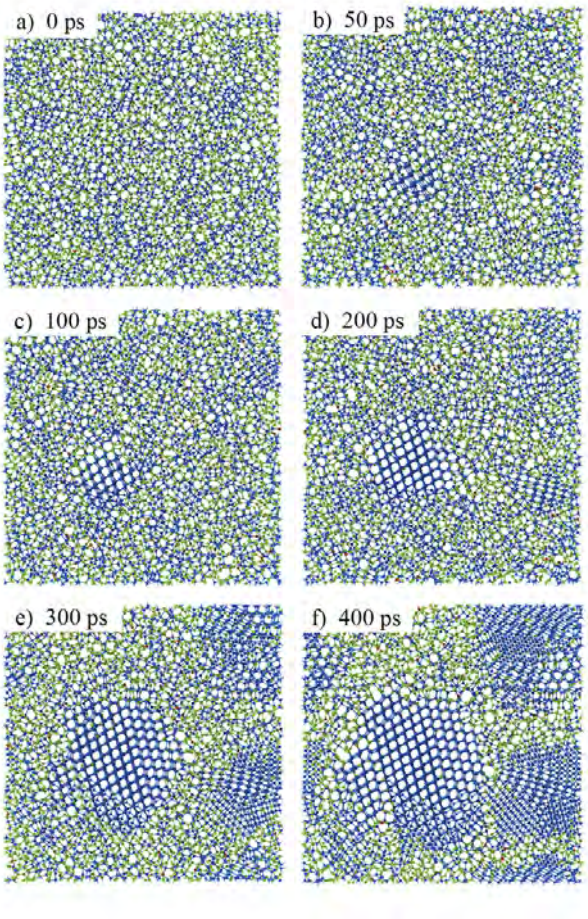

Figure 4. Time evolution during annealing of a 2.8 g/cc amorphous carbon system using S=2.45 Å. Annealing is performed at 6000 K, and the cross-sectional slices are 1 nm in thickness. Red, green, and blue circles depict sp, sp^2, and sp^3 bonding, respectively.

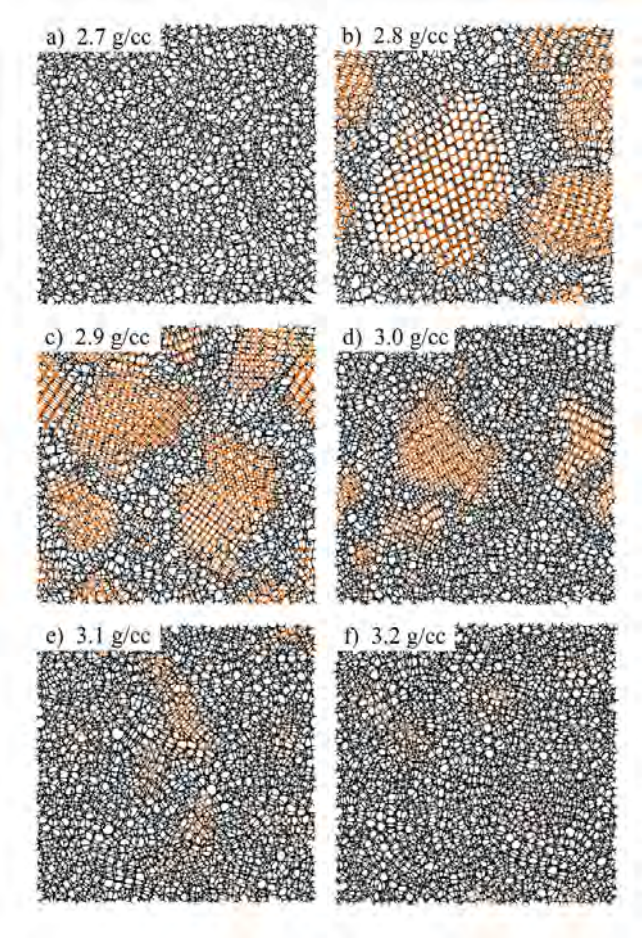

Figure 5. Effect of density on diamond formation in annealing simulations using S=2.45 Å. Atoms with a local diamond topology are shown in orange. All other atoms are shown in black. Annealing is performed at 6000 K and the cross-sectional slices are 1 nm in thickness.

axis aligned along the viewing direction. After 400 ps has elapsed, more than half of the atoms in the viewing plane are blue, and one of the crystallites is nearly half the width of the simulation cell.

To highlight the diamond crystals in a more quantitative manner, we used a coordination-number-based topology tool within OVITO as discussed in the methodology. The results of this analysis are shown graphically in Figure 5, with atoms in a diamond topology shown in orange and all others in black. The figure shows the final structure after 400 ps of annealing for six different densities; all of the data shown used S=2.45 Å. Note that Figure 5(b) can be directly compared to the final panel in Figure 4, with a clear one-to-one correspondence between concentrations of orange in the former and blue atoms in crystallites in the latter. While no distinction is made in the figure between cubic and hexagonal diamond, the cubic phase dominates, typically amounting for around 60% of the diamond atoms. Considering the six densities in Figure 5, it is evident that 2.8 g/cc is some type of threshold, above which diamond crystals can nucleate out of the amorphous structure during annealing. At 2.8 and 2.9 g/cc, the crystallites grow to dominate the simulation cell, while at 3.0 g/cc there is a reduced amount of diamond, diminishing to quite small nanocrystals at 3.1 and 3.2 g/cc. We note that the density range at which the diamond nucleates is far below the experimental diamond density of 3.52 g/cc. This large difference is a warning that the diamond nucleation is unphysical.

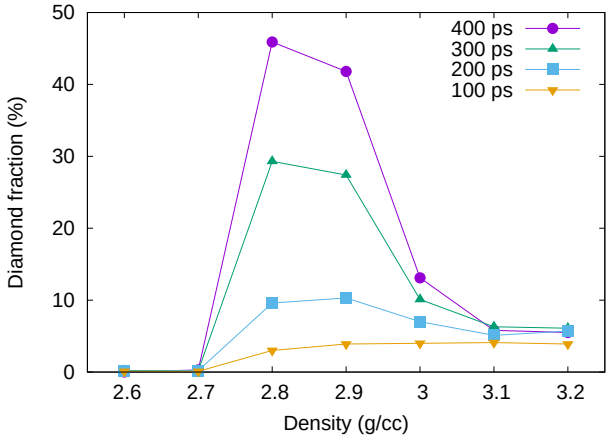

Figure 6. Percentage fraction of atoms in a diamond environment as a function of density at four different times during the annealing. Calculations performed using S=2.45 Å.

The time evolution of the in-growth of the diamond is quantified in Figure 6. At 2.6 and 2.7 g/cc, which is below the critical threshold, no diamond appears anywhere in the structure, but for the optimal densities (2.8 and 2.9 g/cc) the fraction of atoms which are diamond increases to around 45% after 400 ps. At these densities equilibrium has yet to be reached, and the diamond fraction would continue to increase if the simulation were run longer. At the higher densities of 3.1 and 3.2 g/cc, little change occurs after a couple of hundred picoseconds. At these densities, small nanocrystals of diamond nucleate, amounting to around 6% of the total system, but these do not grow in size as occurs at the lower densities.

During the crystallization of the nanocrystals the atoms do not move far from their original positions in the amorphous carbon. Taking the square-root of the MSD for the entire annealing process yields an average displacement of 6.5 Å at 2.8 g/cc, reducing to just 1.6 Å at 3.2 g/cc. This observation that the atoms don't migrate far during the annealing emphasizes how the diamond nucleation occurs locally as atoms rearrange themselves and change their hybridization in order to access a more stable configuration.

In more details, it should be noted that at 2.8 and 2.9 g/cc the pressure of the structure are decreased by passing the time, and by increase an interest thing is that pressure is nearly constant in $S = 2.1, 2.2, 2.3$ and only in our case of study, $S = 2.45$ the pressure is decrease by passing of the time.

Insight into the nature of the diamond crystallites is gained by computing the radial distribution function (RDF), also known as $g(r)$. This information is plotted in Figure 7 for seven densities. At the lower densities the RDF has the characteristic broad peaks of an amorphous material, but at 2.8 and 2.9 g/cc sharp peaks appear superimposed on the broad background, indicative of the diamond phase. Even though diamond crystals can be seen at 3.0 g/cc in Figure 5, these do not produce a clear peak in the RDF, while at the highest densities the RDF resembles that of an amorphous structure.

In addition to highlighting the diamond structure, the RDF also serves to indicate the nature of the diamond itself. The dashed vertical lines in the figure indicate the expected locations of the first three neighbours assuming the ideal (experimental) diamond nearest neighbour distance of 1.547 Å. However, it is apparent that these lines do not coincide with the peaks for the 2.8 or 2.9 g/cc structures. Rather, the peaks at these two densities are instead shifted to larger distances by a fixed multiplicative factor, indicating that the diamond is stretched in both cases. The stretching factors are slightly different for each case, being 1.0375 for 2.8 g/cc and 1.0297 for 2.9 g/cc. The peaks corresponding to these stretched diamond distances are shown as solid vertical lines. Note

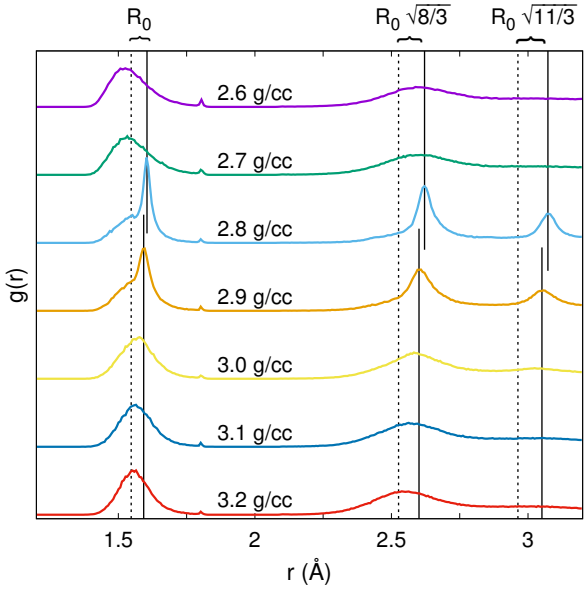

Figure 7. Radial distribution function after annealing for seven different densities using S=2.45 Å. The dashed vertical lines indicate the position of the first three neighbours in ideal (experimental) diamond, while the solid lines indicate the corresponding positions of stretched diamond as described in the text. The geometric factors at the top of the figure relate higher-order neighbours to the nearest neighbour distance R_0.

that only the first peak position is fitted to the data, while the position of the second and third peaks is computed using the geometric factors for the distances in diamond. As expected, the computed position of the second and third peaks corresponds exactly with the peaks in the RDF. This stretching of the diamond reduces the density of the nanocrystals to 3.15 and 3.22 g/cc for the systems with overall density of 2.8 and 2.9 g/cc, respectively. By comparison, the density of ideal diamond is 3.52 g/cc. This stretching in part reflects the tension that the crystals experience due to being embedded in a matrix with a density much lower than diamond itself.

To understand how the appearance of stretched diamond relates to the cutoff itself, quenching and annealing simulations at 2.8 g/cc were performed with four different cutoffs. The RDFs for both the amorphous and annealed samples are presented in Figure 8, along with the associated cutoff function which is plotted in red using the right-hand axis. For the lowest three values of S the RDF of the amorphous and annealed structures are virtually identical, consistent with the behaviour of the unmodified potential in which the annealed structures remain amorphous. Only for the highest value of S=2.45 Å does the RDF develop the sharp peaks indicative of the appearance of the diamond crystallites. This demonstrates conclusively that the appearance of the diamond upon annealing is not a physical effect, but instead is an artifact of the modified potential itself.

The origin of the problem can be understood intuitively via the inset shown in Figure 8(e) which plots both of the RDFs and the cutoff function for the small region indicated in panel (d). This distance range corresponds to the onset of the second neighbour peak as well as the distance at

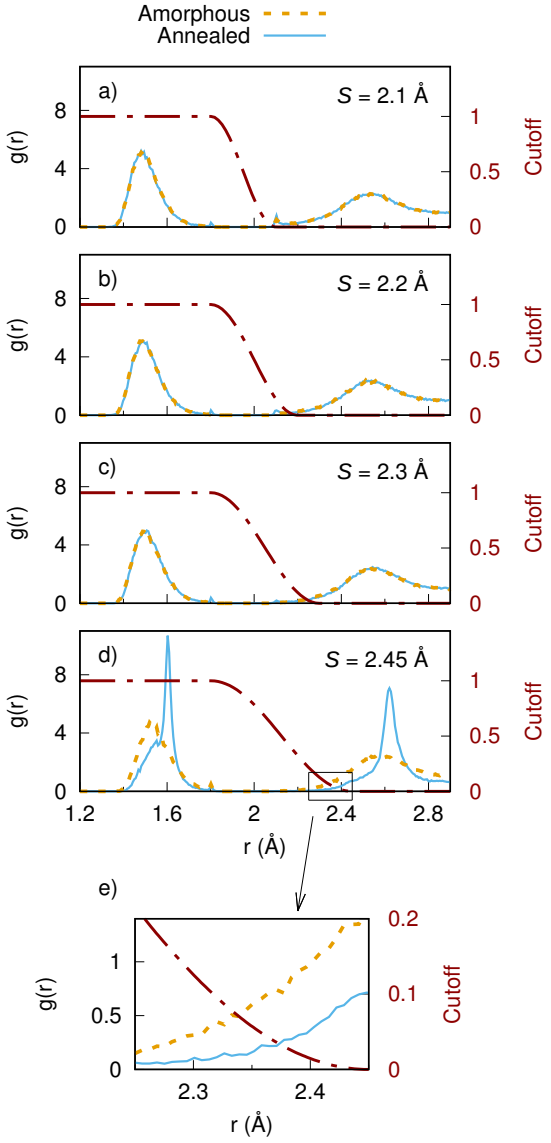

Figure 8. (a-d) Effect of the cutoff parameter S on the radial distribution function of amorphous carbon (gold dotted line) and annealed carbon (solid blue line). The corresponding cutoff function is shown in red using a dash-dot line. Panel (e) shows an inset as indicated for the case S=2.45 Å.

which the cutoff function is decaying away to zero. The inset shows how there is considerable overlap between the tail of the cutoff function and the leading edge of the second RDF peak of the amorphous structure. However, after annealing the RDF has shifted significantly and there is much less overlap with the cutoff function. Inspection of the other three cases shows that this effect is unique to the case S=2.45 Å. For small values of S the cutoff function either terminates

completely prior to the onset of second neighbour distances, or has minimal overlap.

The changes seen in the inset in Figure 8 lie at the heart of the unphysical diamond at large values of S and provide a rationalization for the behaviour. In the Tersoff potential the cutoff function has two roles; (i) it limits the range of the potential to first neighbours only, and (ii) it controls which distances contribute to the bond-order itself. The problems with extending the cutoff arise when there is significantly overlap between the cutoff function and the second neighbour of the RDF. When this happens additional attraction between second neighbours occurs, and the bond order changes such that the effective coordination number increases. Both of these effects combine to stabilise higher coordinated structures, which explains why the amorphous structure, which contains a mixture of sp^2 and sp^3 bonding, gradually transforms into a structure with a much higher fraction of sp^3 bonds.

Since the behaviour is unphysical, we have not explored the reasons why large diamond crystals are not favoured at 3.1 and 3.2 g/cc with S=2.45 Å, but two possible explanation present themselves. One is that the dynamics is simply too slow at 6000 K and higher temperatures are required, but a more plausible rationale is that the stretching of the diamond is an important requirement to avoid interactions between second neighbours, and hence higher densities make the formation of diamond disfavoured as the distances between atoms would be too close to those of ideal diamond itself.

As a final comment, we note that reducing the value of S to avoid the unphysical stablization of diamond is not really a useful option, since reducing S rapidly decreases the sp^3 fraction of the high density amorphous carbon as seen in Figure 3. Since a high sp^3 fraction is the original reason for increasing S, it would appear that this strategy does not have an optimal operational region in which to operate. As an aside, it is interesting to note that in the simulations of Jäger *et al.* [18] which used the REBO potential and increased cutoffs (R=1.95 Å and S=2.25 Å), they too observed an increase in the sp^3 fraction, but at the expense of five-fold coordinated atoms and a large delta-function spike in the RDF. Both of these properties are unphysical, and reinforce the message of this work that the cutoff function of the potential cannot be used as an arbitary tuning parameter, particular for the amorphous carbons where a range of bondlengths are present.

4. Conclusion

In this article we consider the practice of increasing the cutoff of the Tersoff potential to 2.45 Å and show how this modification leads to unexpected behaviour during annealing of amorphous carbon. We demonstrate that diamond nanocrystals nucleate out of the amorphous phase, eventually converting a large portion of the structure. By systematically varying the value of the cutoff and the density, we show that this behaviour is unphysical and arises for numerical reasons associated with interactions between the cutoff function and the second neighbour peak as measured by the radial distribution function. These observations provide an important lesson not only for carbon simulations but for other materials system where there is temptation to tweak parameters to improve a particular property of the potential. The experience of this study is that this practice, while appealing, should be performed with a high degree of caution, and extremely thorough testing should be performed to ensure that the improvement in one property is not offset by a huge reduction elsewhere.

Funding

This work was supported by Australian Research Council Discovery Project DP150103487. NAM acknowledges fellowship FT120100924 and ISM acknowledges fellowship FT140100191. Computational resources are provided by the Pawsey Supercomputing Centre with funding from the

Australian Government and the Government of Western Australia.

References

[1] Tersoff J. Empirical interatomic potential for carbon, with applications to amorphous carbon. Phys Rev Lett. 1988;61:2879–2882.

[2] Abell GC. Empirical chemical pseudopotential theory of molecular and metallic bonding. Phys Rev B. 1985;31:6184–6196.

[3] Brenner DW. Empirical potential for hydrocarbons for use in simulating the chemical vapor deposition of diamond films. Phys Rev B. 1990;42:9458–9471.

[4] de Tomas C, Suarez Martinez I, Marks NA. Graphitization of amorphous carbons: A comparative study of interatomic potentials. Carbon. 2016;109:681–693.

[5] Shenderova OA, Brenner DW, Omeltchenko A, et al. Atomistic modeling of the fracture of polycrystalline diamond. Phys Rev B. 2000;61:3877–3888.

[6] Belytschko T, Xiao SP, Schatz GC, et al. Atomistic simulations of nanotube fracture. Phys Rev B. 2002;65:235430.

[7] Gamboa A, Farbos B, Aurel P, et al. Mechanism of strength reduction along the graphenization pathway. Sci Adv. 2015;1:e1501009.

[8] Grantab R, Shenoy VB, Ruoff RS. Anomalous Strength Characteristics of Tilt Grain Boundaries in Graphene. Science. 2010;330:946–948.

[9] Wei Y, Wu J, Yin H, et al. The nature of strength enhancement and weakening by pentagonheptagon defects in graphene. Nat Mater. 2012;11:759–763.

[10] Zhang B, Mei L, Xiao H. Nanofracture in graphene under complex mechanical stresses. Appl Phys Lett. 2012;101:121915.

[11] Wu J, Wei Y. Grain misorientation and grain-boundary rotation dependent mechanical properties in polycrystalline graphene. J Mech Phys Solids. 2013;61:1421–1432.

[12] He L, Siusiu G, Lei J, et al. The effect of Stone-Thrower-Wales defects on mechanical properties of graphene sheets - A molecular dynamics study. Carbon. 2014;75:124–132.

[13] Zhao H, Aluru NR. Temperature and strain-rate dependent fracture strength of graphene. J Appl Phys. 2010;108:064321.

[14] Cao A, Qu J. Atomistic simulation study of brittle fracture in nanocrystalline graphene under uniaxial tension. Appl Phys Lett. 2013;102:071902.

[15] Jhon YI, Jhon YM, Yeom GY, et al. Orientation dependence of the fracture behavior of graphene. Carbon. 2014;66:619–628.

[16] Dewapriya MAN, Rajapakse RKND, Phani AS. Atomistic and continuum modelling of temperature-dependent fracture of graphene. Int J Fract. 2004;187:199–212.

[17] Rajasekaran G, Kumar R, Parashar A. Tersoff potential with improved accuracy for simulating graphene in molecular dynamics environment. Mater Res Express. 2016;3:035011.

[18] Jäger HU, Albe K. Molecular-dynamics simulations of steady-state growth of ion-deposited tetrahedral amorphous carbon films. J Appl Phys. 2000;88:1129–1135.

[19] Titantah JT, Lamoen D. sp^3/sp^2 characterization of carbon materials from first-principles calculations: X-ray photoelectron versus high energy electron energy-loss spectroscopy techniques. Carbon. 2005; 43:1311–1316.

[20] Sha ZD, Branicio PS, Pei QX, et al. A modified Tersoff potential for pure and hydrogenated diamond-like carbon. Chem Materials Science. 2013;67:146–150.

[21] Nordlund K, Keinonen J, Mattila T. Formation of Ion Irradiation Induced Small-Scale Defects on Graphite Surfaces. Phys Rev Lett. 1996;77:699–702.

[22] Marks NA. Evidence for subpicosecond thermal spikes in the formation of tetrahedral amorphous carbon. Phys Rev B. 1997;56:2441–2446.

[23] Plimpton S. Fast parallel algorithms for short-range molecular dynamics. J Comput Phys. 1995;117:1–19.

[24] Maras E, Trushin O, Stukowski A, et al. Global transition path for dislocation formation in Ge on Si(001). Comput Phys Commun. 2016;205:13–21.

[25] Stukowski A. Visualization and analysis of atomistic simulation data with OVITO - the Open Visualization Tool. Model Simul Mater Sc. 2010;18:015012.
[26] Bussi G, Donadio D, Parrinello M. Canonical sampling through velocity rescaling. J Chem Phys. 2007; 126:014101.
[27] Schwan J, Ulrich S, Roth H, et al. Tetrahedral amorphous carbon films prepared by magnetron sputtering and dc ion plating. J App Phys. 1996;79:1416–1422.